Volume 12
Number 42
14 November 2021
Pages 6043-6190

Polymer Chemistry

rsc.li/polymers

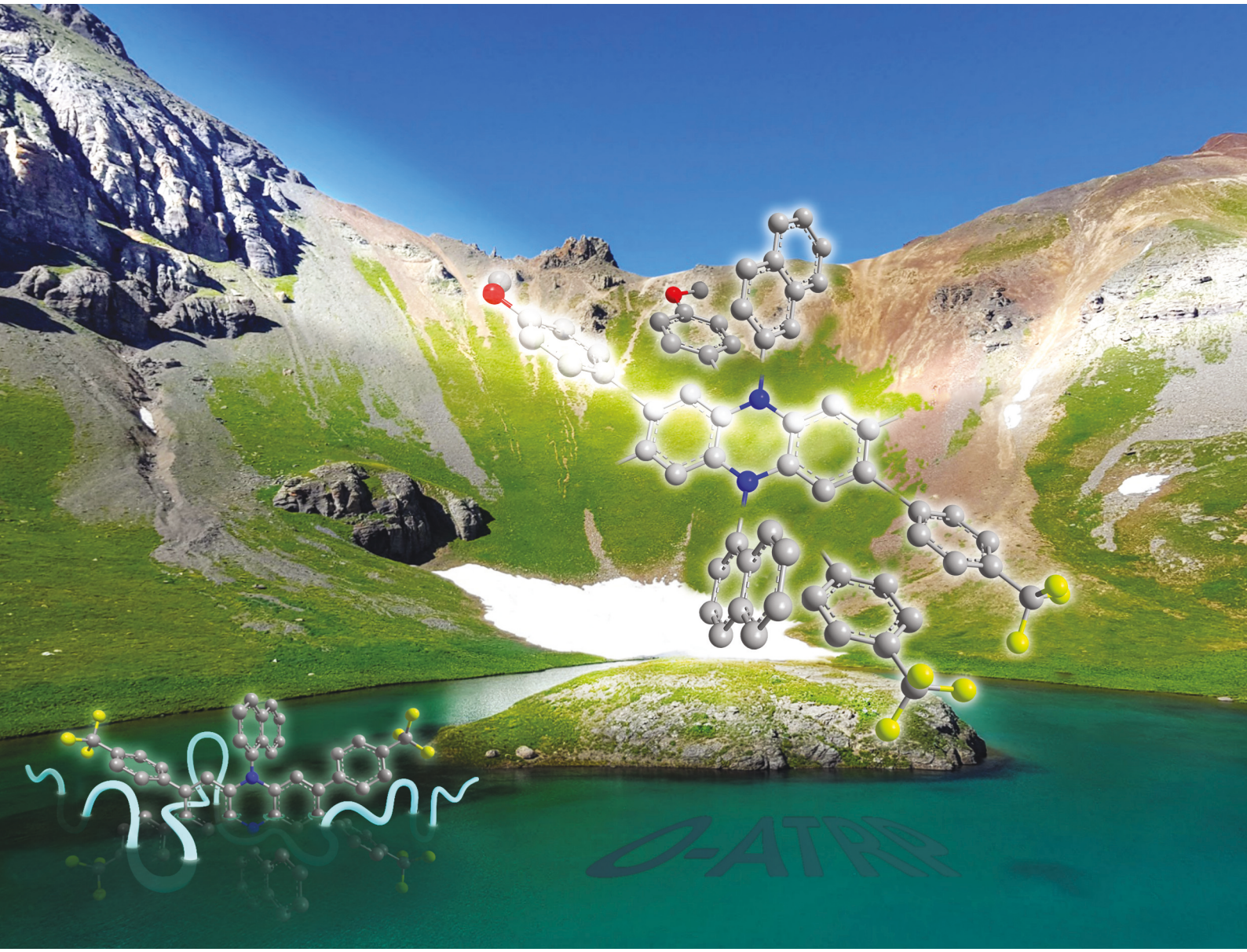

ISSN 1759-9962

ROYAL SOCIETY OF CHEMISTRY

PAPER

Garret M. Miyake *et al.*

Structure–property relationships of core-substituted diaryl dihydrophenazine organic photoredox catalysts and their application in O-ATRP

Polymer Chemistry

ROYAL SOCIETY OF CHEMISTRY

PAPER

View Article Online
View Journal | View Issue

Cite this: *Polym. Chem.*, 2021, **12**, 6110

Structure–property relationships of core-substituted diaryl dihydrophenazine organic photoredox catalysts and their application in O-ATRP†

Mariel J. Price, Katherine O. Puffer, Max Kudisch, Declan Knies and Garret M. Miyake *

Photoinduced organocatalyzed atom-transfer radical polymerization (O-ATRP) is a controlled radical polymerization technique that can be driven using low-energy, visible light and makes use of organic photocatalysts. Limitations of O-ATRP have traditionally included the need for high catalyst loadings (1000 ppm) and the narrow scope of monomers that can be controllably polymerized. Recent advances have shown that *N*,*N*-diaryl dihydrophenazine (DHP) organic photoredox catalysts (PCs) are capable of controlling O-ATRP at PC loadings as low as 10 ppm, a significant advancement in the field. In this work we synthesized five new DHP PCs and examined their efficacy in controlling O-ATRP at low ppm catalyst loadings. We found that we were able to polymerize methyl methacrylate at PC loadings as low as 10 ppm (relative to monomer) while producing polymers with dispersities as low as $Đ$ = 1.33 and achieving initiator efficiencies (I^*) near unity (102%). In addition to applying these PCs in O-ATRP, we carried out a thorough investigation into the structure–property relationships of the new DHP PCs reported herein and report new photophysical characterization data for previously reported DHPs. The insight into the DHP structure–property relationships that we discuss herein will aid in the elucidation of their ability to catalyze O-ATRP at low catalyst loadings. Additionally, this work sheds light on how structural modifications affect certain PC properties with the goal of bolstering our understanding of how to tune PC structures to overcome current limitations in O-ATRP such as the controlled polymerization of challenging monomers.

Received 8th August 2021,
Accepted 21st September 2021

DOI: 10.1039/d1py01060c

rsc.li/polymers

Introduction

The development of organic photoredox catalysts (PCs) has revolutionized the way that chemists can approach both small molecule and macromolecular syntheses.[1–5] Establishing structure–property relationships of organic PCs is essential for guiding the development of new PCs with targeted properties and to increase their use and application in new chemical transformations. One specific application that knowledge of structure–property relationships in PCs has been leveraged for is organocatalyzed-atom transfer radical polymerization (O-ATRP). O-ATRP is a reversible-deactivation radical polymerization (RDRP) technique that employs the energy of visible light to synthesize polymers with controlled molecular weights and architectures (Fig. 1). In RDRPs, successful control over the polymerization is typically assessed by the ability to produce polymers with low dispersity ($Đ$) ($Đ$ < 1.5), targeted molecular weights, and retention of predictable polymer chain end groups. O-ATRP was developed as an alternative to traditional metal catalyzed atom transfer radical polymerization (ATRP), one of the most widely used RDRP techniques. O-ATRP offers certain advantages over traditional metal catalyzed ATRP in that it enables the synthesis of polymers free of metal con-

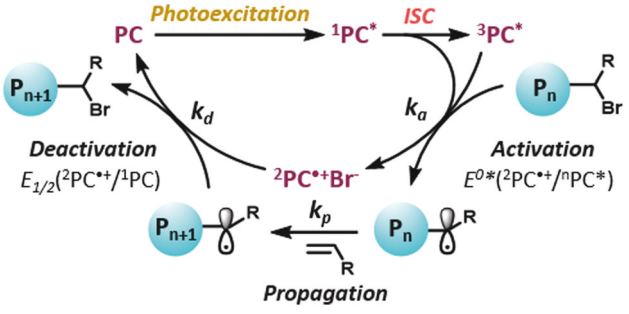

Fig. 1 Proposed mechanism for O-ATRP.

Department of Chemistry, Colorado State University, Fort Collins, CO 80523-1872, USA. E-mail: garret.miyake@colostate.edu

†Electronic supplementary information (ESI) available. See DOI: 10.1039/d1py01060c

taminants. Without metal contamination, polymers synthesized *via* O-ATRP can more readily be used for metal sensitive applications such as in electronics or biomedical technologies.[3] From a sustainability perspective, O-ATRP utilizes a readily abundant source of energy (light) to drive a useful chemical reaction. Although non-organic catalysts have also been developed for visible light-driven ATRP,[4,6,7] they necessitate the use metals such as copper, ruthenium, or iridium which limits the potential applications of the polymers, as highlighted above. Furthermore, concerns about the sustainability of using precious metals such as iridium motivate use of organic PCs.[8]

Our research group has worked in the development of different families of highly reducing PCs originally tailored for O-ATRP, including *N*-aryl phenoxazines,[9–11] *N*,*N*-diaryl dihydrophenazines (DHPs),[12–17] *N*-aryl phenothiazines,[18] and *N*-aryl dimethyl dihydroacridines[19] all of which are comprised solely of atoms with high natural abundance, further bolstering their prowess as sustainable catalysts.

Significant advances have been made toward increasing our understanding of the impact of certain PC properties on specific steps of the proposed O-ATRP mechanism.[20–24] Simultaneous with the advancements in our understanding of relevant PC properties has been growth in our understanding of the intricacies of the proposed O-ATRP mechanism.[24] Here, we discuss a distilled version of the proposed mechanism for O-ATRP (Fig. 1). In the first step of O-ATRP, a PC is photoexcited *via* irradiation. The excited state PC (^{n}PC*) reduces either the alkyl halide initiator *via* a single electron transfer reaction to initiate polymerization or, once the polymerization has been initiated, reduces the halide-capped polymer chain end to re-activate polymerization. The rate of activation is defined as k_a. Reduction of the initiator/halide-capped polymer chain end yields a carbon-centered radical on the initiator/polymer chain end which can propagate through a reaction with monomer leading to polymerization. The rate of polymerization is defined as k_p. Reduction of the alkyl halide initiator or halide-capped polymer chain end also generates the oxidized PC species (^{2}PC$^{\bullet+}$) and a halide anion (X^-) which we propose to form an ion pair.[25] This ion pair (PC$^{\bullet+}$X$^-$) is proposed to deactivate the carbon centered radical on the chain end group of the growing polymer through reinstallation of the halide; the rate of deactivation is described as k_d. Deactivation yields both the halide-capped polymer and ground state PC. Key to the success of ATRP and O-ATRP is that k_d is faster than k_a. Rapid deactivation of the radical on the end group of the growing polymer chain controls the concentration of radicals and helps minimize bimolecular radical termination reactions, which are counterproductive to the synthesis of polymers with controlled molecular weights.

There are several thermodynamic requirements that PCs used to catalyze O-ATRP through an oxidative quenching cycle (Fig. 1) must meet. The reduction potential of the excited state PC (E^{o*}(^{2}PC$^{\bullet+}$/^{n}PC*)) must be reducing enough (~−0.6 to −0.8 V *vs.* SCE) to reduce both the alkyl halide bond of the initiator or the polymer chain end.[12] Additionally, the ion pair of ^{2}PC$^{\bullet+}$ and X^- must be sufficiently oxidizing to deactivate the growing polymer chain (~−0.8 V) to reinstall the halide. There are also several photophysical PC properties that are relevant to the O-ATRP mechanism (Fig. 2). Absorption of visible light (400 nm–700 nm) enables the use of visible light to selectively stimulate photoexcitation of the PC. This attribute is desirable as use of ultraviolet (UV) light can cause unwanted side reactions due to the ability of many small molecules, including monomers used in O-ATRP, to absorb UV light. PCs that possess a high molar extinction coefficient ($\varepsilon_{max,abs}$) at the wavelength used for photoexcitation are preferred as PCs with higher $\varepsilon_{max,abs}$ are more efficient at absorbing light and therefore accessing the reactive excited state ^{n}PC*, which at higher concentrations can lead to more efficient and uniform activation in O-ATRP as well as be more resilient to differences in irradiation intensity. Upon photoexcitation, the PC is promoted to some singlet excited state (S_n) (Fig. 2) from which it relaxes to the lowest S_1 energy state. From S_1 the PC, considered to be in the lowest energy singlet excited state (^{1}PC*), can relax back to the ground state *via* a radiative pathway (fluorescence) or non-radiative pathway (Fig. 2), can react with a substrate *via* electron-transfer or energy transfer, or can undergo intersystem crossing to access the triplet excited state (T_1). The PC in the triplet excited state (^{3}PC*) most commonly reacts with some substrate or *via* a radiative decay pathway (phosphorescence) or *via* non-radiative decay return back to the ground state (S_0) (Fig. 2). Both ^{1}PC* and ^{3}PC* are highly reducing for the PCs discussed in this work and are likely responsible for activation in O-ATRP, though their individual contributions to activation is dependent on reactant concentrations and photophysical properties.[20] As triplet excited state lifetimes (τ_{T1}) are longer than singlet excited states life-

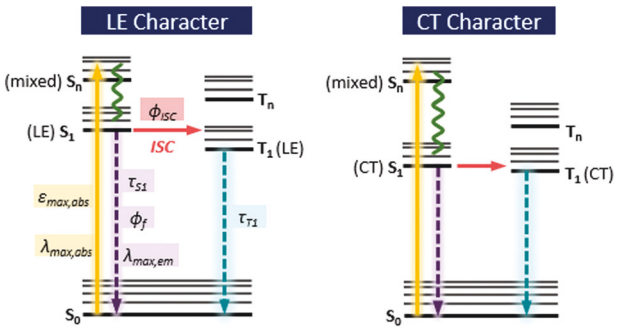

Fig. 2 Jablonski diagrams representing PCs that form excited states with either local excitation (LE) character (left) or charge transfer (CT) character (right) in their lowest photoexcited states. Solid yellow arrow indicates photoexcitation from S_0 to S_n to form photocatalyst in the singlet excited state (^{1}PC*). Purple and blue dashed arrows represent radiative decay from the lowest energy singlet excited state (S_1) and the lowest energy triplet excited state (T_1), or fluorescence and phosphorescence, respectively. Pink arrow represents inner system crossing (ISC) from S_1 to T_1 to form photocatalyst in the triplet excited state (^{3}PC*). Green waved line represents internal conversion (IC). PC properties associated with each type of aforementioned transition are labeled adjacent to those transitions in the Jablonski diagram on the left.

times (τ_{S1}) and are therefore more likely to engage in a bimolecular interaction, ^{3}PC* is commonly attributed as the species responsible for activation. However, recent studies have shown that there are several factors that can influence the ratios of ^{1}PC* and ^{3}PC* responsible for activation in O-ATRP such as the concentration of initiator used,[20] the solvent that the polymerization is conducted in,[22] and electron transfer rates influenced by the PC structure.[21] As ^{n}PC* is responsible for activation, it is important to understand how the structure of the PC influences the nature of ^{n}PC*. DHP PCs that access charge-transfer (CT) type excited states have been shown to be more effective PCs in controlling O-ATRP.[13] In CT PCs, photoexcitation triggers a shift in electron density from one part of the molecule (the donor) to another part (the acceptor) generally resulting in a more-polar and stabilized excited state (Fig. 2). The specific role of CT in improving PC control in O-ATRP is still debated.[11,23,26,27]

In previous work, core-extension of *N*-aryl phenoxazines, DHPs, and *N*-aryl dimethyl dihydroacridines has been shown to significantly impact PC properties and improved control in O-ATRP.[11,14–17,19] Prior work on aryl core-extended DHPs explored how core-extension of a particular DHP (which possessed an electron withdrawing 4-trifluoromethylphenyl *N*-aryl group) impacted PCs properties and control in O-ATRP (Fig. 3).[14] Importantly, the aryl-core extended DHPs were shown to control O-ATRP at catalyst loadings as low as 10 ppm, producing polymers with controlled molecular weights ($Đ$ < 1.42) while achieving I^* > 90%.[14] The application of PCs at low ppm (<1000 ppm) was a significant advancement in the field of O-ATRP. The ability to control polymerizations at low PC loadings is beneficial both from a sustainability perspective and from a practical standpoint as low ppm PC loadings limits contamination of the polymers by the PC. In this work, we sought to further investigate structure–property relationships in core-extended DHPs first, to gain insight into the properties that enable them to control O-ATRP at low ppm PC loadings and second, because deeper understanding of structure–property relationships in PCs can help direct the development of new PCs with properties that can help overcome current limitations in O-ATRP (Fig. 3). Herein, we demonstrate the synthesis and characterization of five new core-extended DHP PCs, examine the structure–property relationships in those PCs, and investigate their ability to control the polymerization of acrylate and methacrylate monomers in O-ATRP. Furthermore, we provide new photophysical characterization data for previously reported DHPs and test their ability to control O-ATRP at low ppm PC loadings for the first time.

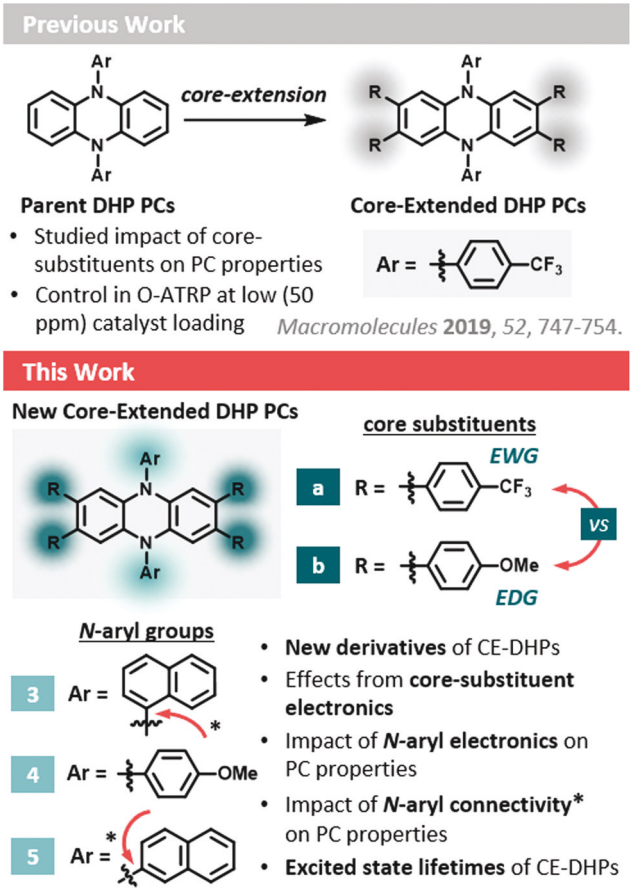

Fig. 3 Previously reported work on core-extended DHPs (top). Focus of this work and structures for new core-extended DHPs developed in this work (bottom). *Different points of connectivity for naphthalene *N*-aryl group to DHP PC are indicated by red arrows.

Results and discussion

Synthesis of PCs

The synthesis of core-extended DHPs involves several steps beginning with the reduction of phenazine (**1**) to dihydrophenazine (**2**) (Fig. S3†).[28] Following the synthesis of dihydrophenazine (**2**), Buchwald–Hartwig C–N cross coupling conditions are used to access the parent (non-core extended) DHP PCs **3**, **4**, and **5**. PC **5** was synthesized using C–N coupling conditions employed by our group for the synthesis of PCs **3**, **4**, and **5**, when we first reported the use of these PCs for O-ATRP in 2016.[12] Unfortunately, under these previous conditions the yield reported for PC **3** was only 3%.[12] In this work, we explored other C–N cross coupling conditions for the synthesis of PC **3** that were previously reported for the synthesis of 2-naphthyl-10-phenoxazine.[11] Using bis(dibenzylideneacetone) palladium(0) ($Pd(dba)_2$) and tri-*tert*-butyl phosphine ($P(tBu)_3$) for the C–N cross coupling of dihydrophenazine (**2**) and 1-bromonaphthalene (instead of RuPhos and RuPhos precatalyst), we observed an improved yield of PC **3** (57%). PC **4** was also synthesized using $Pd(dba)_2$ and $P(tBu)_3$. Core-extension of PCs **3**, **4**, and **5** was accomplished by first brominating the DHP core (utilizing previously reported methods for the synthesis of core-extended DHPs)[14] then through a Suzuki–Miyaura C–C cross-coupling reaction with the brominated DHP and the boronic acid of a phenyl substituent with either an electron withdrawing group (**a**) or an electron donating group (**b**) (Fig. 3). Non-core-extended DHPs (or "parent DHPs") discussed

in this work include PCs **3**, **4**, and **5** which have *N*-aryl group **3**, **4**, or **5**, respectively (Fig. 3). Core-extended DHPs discussed in this work include PCs **3a**, **4a**, and **5a** (which have electron withdrawing core substituent **a** and *N*-aryl group **3**, **4**, or **5**, respectively, as well as PCs **3b** and **5b** which have electron donating core substituent **b** and either *N*-aryl group **3** or **5**, respectively.

Photophysical characterization

To study the photophysical properties of the core-extended DHPs, we employed a combination of spectroscopic techniques and computational approaches. First, we sought to probe how the *N*-aryl group and core substituents in core-extended DHPs impact photophysical PC properties (specifically the $\lambda_{max,abs}$, $\varepsilon_{max,abs}$), the ability to access CT states, the excited state energies (E_{S1} & $E_{T1,comp}$), quantum yield of fluorescence (ϕ_f), and the excited state lifetimes (τ_{S1} & τ_{T1}).

Absorption. We hypothesized that core-extension would generally lead to a red-shift in the $\lambda_{max,abs}$ through stabilization of the π* orbitals involved in photoexcitation, but were uncertain how the electron withdrawing or donating character of the core substituents might influence $\lambda_{max,abs}$. In previous studies where structure–property relationships of PCs with donor–acceptor structures similar to core-extended DHPs reported herein were examined (*i.e.*: *N*-aryl phenoxazines,[11] *N*,*N*-diaryl dihydrophenazines,[14] and *N*-aryl dimethyl dihydroacridines[19]), core-extension was shown to red-shift $\lambda_{max,abs}$. We observed that core-extension does lead to a red-shifted $\lambda_{max,abs}$ for these PCs (Table 1), however there appeared to be little to no notable effect on $\lambda_{max,abs}$ imparted by the electron withdrawing or electron donating character of the core-substituent. The $\lambda_{max,abs}$ for **3a** ($\lambda_{max,abs}$ = 385 nm) and **3b** ($\lambda_{max,abs}$ = 385 nm) were experimentally determined to be identical and the $\lambda_{max,abs}$ of **5a** ($\lambda_{max,abs}$ = 373 nm) and **5b** ($\lambda_{max,abs}$ = 371 nm) are separated by only 2 nm. In contrast to the core substituents, the identity of the *N*-aryl group has a notable impact on $\lambda_{max,abs}$. The $\lambda_{max,abs}$ red-shifts by ~12 nm when the *N*-aryl group on CE-DHPs is changed from 2-naphthylene (PCs **5a** and **5b**) to 1-naphthalene (PCs **3a** and **3b**). Additionally, exchanging a naphthalene *N*-aryl group for an electron donating *N*-aryl group (4-methoxyphenol) results in a red-shift from 7 to 19 nm (PC **4a**: $\lambda_{max,abs}$ = 392 nm). Of the core-extended DHPs that have been reported, **4a** has the highest measured $\lambda_{max,abs}$ (392 nm).[14]

Though the identity of the core substituents has little measurable effect on $\lambda_{max,abs}$, the molar absorptivity at $\lambda_{max,abs}$ ($\varepsilon_{max,abs}$) is significantly impacted by the electronics of the core substituent (Fig. 4). We hypothesized that, in accordance with previous work, $\varepsilon_{max,abs}$ would increase with core-extension as a result of extended conjugation of the PC core. Indeed, the measured $\varepsilon_{max,abs}$ values are between 7000 and 21 700 M^{-1} cm^{-1} larger for core-extended PCs than non-core-extended parent PCs. The measured increase in efficiency of photon absorption in core-extended PCs is corroborated by oscillator strength (f) values predicted using time-dependent density functional theory calculations (TD-DFT) (Fig. 4B & Fig. S61–S69†). The predicted f values shown in Fig. 3 and Fig. S61–S69† approximate the strength of a certain electronic transition, in this case a π–π* transition. Furthermore, we found that the $\varepsilon_{max,abs}$ of PCs core-extended with the EWG **a** are significantly higher than the $\varepsilon_{max,abs}$ for PCs core-extended with EDG **b**. Specifically, the $\varepsilon_{max,abs}$ measured for **3a** ($\varepsilon_{max,abs}$ = 22 200) is 8800 M^{-1} cm^{-1} greater than the $\varepsilon_{max,abs}$ of **3b** ($\varepsilon_{max,abs}$ = 13 100) and the measured $\varepsilon_{max,abs}$ of **5a** ($\varepsilon_{max,abs}$ = 27 600) is 11 400 M^{-1} cm^{-1} higher than for **5b** ($\varepsilon_{max,abs}$ = 15 900). To explore potential factors that contribute to the significant difference in $\varepsilon_{max,abs}$ between PCs **3a**, **4a**, and **5a** *vs.* PCs **3b** and **5b**, we used TD-DFT. The electronic transitions with the highest predicted oscillator strengths in PCs **3a**, **4a**, and **5a**, are predicted to occur between a π_{HOMO} centered on the PC core and a π_{LUMO+n} spread across the PC core and all four core-substituents (Fig. 4B & Fig. S65, S66†). In contrast to PCs **3a**, **4a**, and **3b**, the electronic transitions with the highest predicted oscillator strengths for PCs **3b** and **5b** are forecasted to occur between a π_{HOMO} centered on the PC core and a π_{LUMO+n} spread across the core and both *N*-aryl substituents (Fig. 4B and Fig. S69†). Interestingly, the π_{LUMO+n} predicted to have greater involvement in absorption resides more heavily on the core of **3b** than it does for **5b**. Our understanding is

Table 1 Photophysical properties of PCs investigated in this study

PC	$\lambda_{max,abs}$ [a] (nm)	$\varepsilon_{max,abs}$ [b] (M^{-1} cm^{-1})	$\lambda_{max,em}$ [c] (nm)	Stokes shift (nm)	$E_{S1,exp}$ [d] (eV)	$E_{T1,comp}$ [e] (eV)	ϕ_f [f] (%)	τ_{S1} [g] (ns)	τ_{T1} [h] (μs)
3	362	6100	663	297	1.87	2.23	1.32	9	0.63
3a	385	22 200	586	201	2.12	1.91	9.00	17	144
3b	385	13 100	636	251	1.95	2.07	4.31	11	42
4	373	5200	467	94	2.66	2.29	23.0	37	88
4a	392	20 900	599	207	2.07	1.82	36.0	13	—[i]
5	343	5900	654	311	1.90	2.19	0.72	—[j]	3.5
5a	373	27 600	587	214	2.11	1.89	35.0	17	—[i]
5b	371	15 900	621	250	2.00	1.99	4.00	11	108

[a] Maximum wavelength of absorption was measured using UV-Vis in DMAc. [b] Molar absorptivity calculated at λ_{max} in DMAc. [c] Maximum wavelength of emission was measured using steady-state fluorescence spectroscopy in DMAc. [d] Singlet energies were calculated using the maximum wavelength of emission (E(eV) = 1239.8/λ (nm)). [e] DFT calculations were performed at the uM06/6-311+G(d,p)//uM06/6-31+G(d,p) level of theory with CPCM-described solvation in DMAc. [f] Quantum yield of fluorescence was measured in DMAc using absolute methods. [g] Singlet excited state lifetime was determined by kinetic emission. [h] Triplet excited state lifetime was determined by kinetic absorption. [i] No triplet signal detected. [j] Singlet excited state lifetime was too short to measure as it was below the detection limit of the instrument.

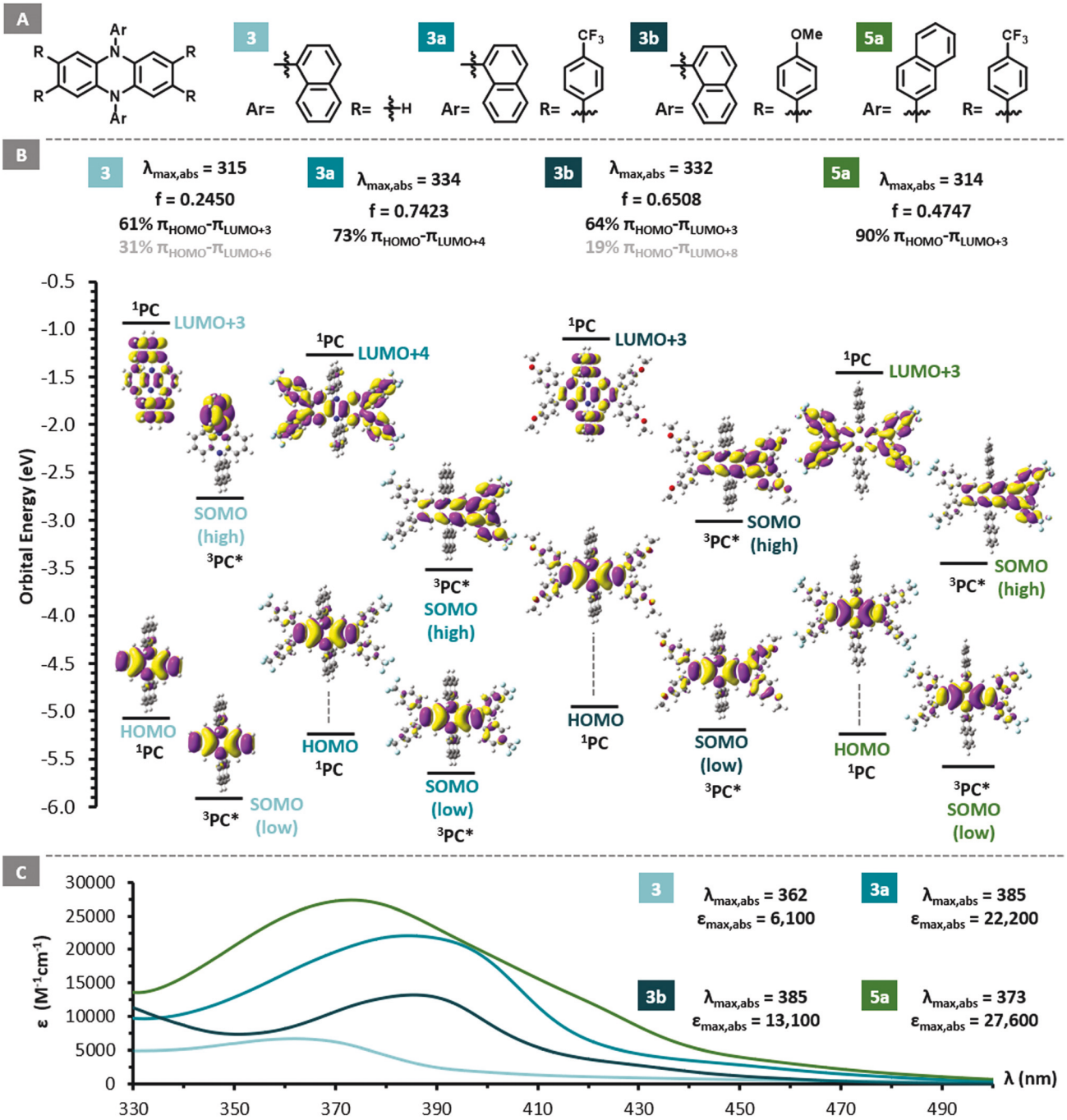

Fig. 4 (A) Structures of PCs discussed in this figure. (B) Results from time-dependent density functional theory (TD-DFT) calculations of orbitals involved in excitation of PCs **3**, **3a**, **3b**, and **5a** at the predicted $\lambda_{max,abs}$ (top) and visualized molecular orbitals predicted to be involved in photoexcitation (bottom). (C) UV-vis spectra of PC **3**, **3a**, **3b**, and **5a** acquired in *N*,*N*-dimethylacetamide (DMAc) with observed maximum wavelength of absorption ($\lambda_{max,abs}$) in units of nm and molar extinction coefficient ($\varepsilon_{max,abs}$) in units of M^{-1} cm^{-1} shown.

that all the core-extended DHPs are predicted to access a mixed excited state upon initial photoexcitation where charge transfer (CT) is not fully delocalized to the *N*-aryl group or the core-substituents, but nor is the nature of the excited state purely of locally excited (LE) character. Considering the differences in where π_{LUMO+n} is predicted to reside for PCs **3a**, **4a**, and **5a** *vs.* for **3b** and **5b**, we postulate that the location of π* orbitals on the PC could influence the efficiency of photon absorption accounting for the difference in $\varepsilon_{max,abs}$ that we observed for core-extended DHPs with different core-substituents but the same *N*-aryl group, although further investigations are necessary to further support this hypothesis.

Though there is a measurable change in the $\varepsilon_{max,abs}$ for CE-DHPs with different *N*-aryl groups, the shifts are of a lesser

magnitude than for those observed from changing electron donating core substituents to electron withdrawing core substituents on PCs with the same *N*-aryl group. **4a** has the lowest $\varepsilon_{max,abs}$ of **3a**, **4a**, and **5a**, but only ~1300 M^{-1} cm^{-1} lower than **3a**. Of all the CE-DHPs investigated here, **5a** has the highest molar extinction coefficient at $\varepsilon_{max,abs}$ ~ 27 600 M^{-1} cm^{-1}.[14] Despite the measured $\varepsilon_{max,abs}$ of **5a** being ~5400 M^{-1} cm^{-1} higher than **3a**, TD-DFT calculations predicted the $\varepsilon_{max,abs}$ to be highest for **3a** and lowest for **5a** (Fig. 4C).

Charge transfer. A combination of DFT and experimental approaches were used to examine the nature of PC*. Studies of non-core extended DHPs support access to a CT excited state located primarily on the naphthalene *N*-aryl substituent for PCs **3** and **5**[25] and that the connectivity of the *N*-naphthalene group, specifically in *N*-aryl phenoxazines, does have an impact on CT.[26] In this work, we sought to investigate how core-extension and the *N*-aryl group impact CT in core-extended DHP PCs. First, we used fluorescence spectroscopy to measure the maximum emission wavelength ($\lambda_{max,em}$) and emission profile of parent and core-extended PCs (Table 1). For all the PCs, except PC **4**, we observed broad and featureless emission profiles suggesting that these PCs access a CT state for ^{1}PC*. We then used the measured $\lambda_{max,em}$ to calculate the Stokes shift ($\Delta\lambda$) for each PC [$\Delta\lambda = \lambda_{max,em}$ (nm) − $\lambda_{max,abs}$ (nm)]. We observed that $\Delta\lambda$ for PCs **3** and **5** decreases as a result of core-extension (Table 1). Interestingly, core-extension of PC **4** ($\Delta\lambda$ = 94 nm) to PC **4a** ($\Delta\lambda$ = 207 nm) results in a 113 nm increase in $\Delta\lambda$, suggesting that through specific core-modifications, parent DHPs that do not possess CT character can be modified to enable access to a CT state. As there is previous work supporting that core-extended *N*-aryl phenoxazines and *N*,*N*-diaryl dihydrophenazines can access a CT state located on the core substituents,[11,14] we hypothesized that core-extension with EWG **a** would increase the $\Delta\lambda$ of PCs **3a** and **5a** relative to PCs with EDG **b** (**3b** and **5b**). To the contrary, we observed that the $\Delta\lambda$ of PCs **3a** ($\Delta\lambda$ = 201 nm) and **5a** ($\Delta\lambda$ = 214 nm) was significantly less than for PCs **3b** ($\Delta\lambda$ = 251 nm) and **5b** ($\Delta\lambda$ = 250 nm). In addition to examining the Stokes shift, CT character can be assessed for ^{n}PC* by investigating solvatochromism, where the PC is dissolved in solvents of increasing polarity then photoexcitation *via* irradiation reveals how the energy of emission from polarized ^{n}PC* is stabilized by solvents of increasing polarity resulting in a lower energy (red-shifted) emission (Fig. 5B and Fig. S46–S53†). Solvatochromism of **3b** and **5b** appear more extensive than solvatochromism of **3a** and **5a** supporting our observation that the former have a larger $\Delta\lambda$.

DFT calculations were also used to probe the CT character of PCs in the ground state and of ^{3}PC*. Generation and visualization of singly occupied molecular orbitals (SOMOs) of the parent and core-extended ^{3}PC* species show some degree of spatial separation between the low-lying SOMOs and high-lying SOMOs (Fig. 5B & Fig. S70–S72†). For core-extended PCs, the high-lying SOMO of ^{3}PC* is predicted to be distributed across the core and two of the core substituents whereas the low-lying SOMO is predicted to reside centered primarily on the core of ^{3}PC* (Fig. 5B and Fig. S70–72†). Interestingly, there is minimal observable difference between the nature of the high lying SOMOs for **3b** and **3a** or between **5b** and **5a**.

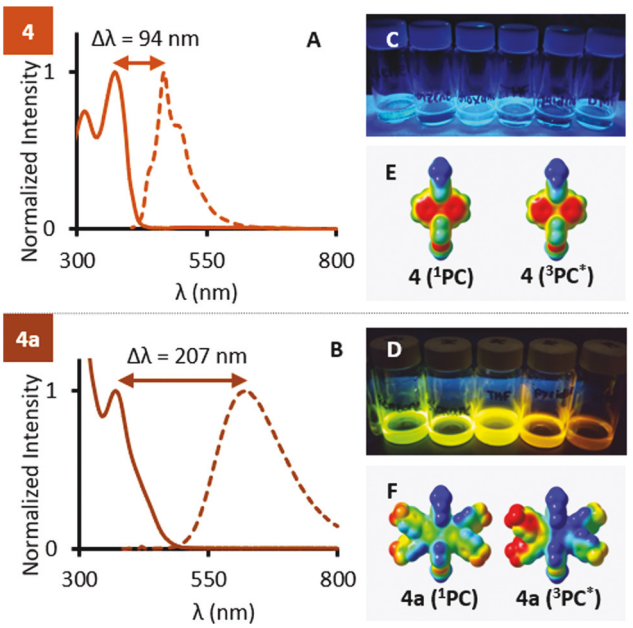

Fig. 5 (A & B) Normalized absorption (solid) and emission (dashed) spectra of PCs **4** and **4a**, respectively, with Stokes shift shown in nm. (C & D) Photographs of PCs **4** and **4a** in solvents of increasing polarity from left to right while being irradiated with 365 nm light. (E & F) Electrostatic potential (ESP) maps (generated using DFT) showing areas of high electrostatic potential (red) and low electrostatic potential (blue) for the PC in the singlet ground state (left) and in the triplet excited state (right).

Excited state absorption spectra of ^{3}PC* for core-extended DHPs were measured using time-resolved (TA) spectroscopy. The spectral signals were followed at a single wavelength over time to obtain kinetic data which was then used to determine triplet excited state lifetimes for the PCs. When comparing spectral absorption traces (Fig. 6) of PCs with the same core substituent (*i.e.* **3b** and **5b**) and PCs with the same *N*-aryl

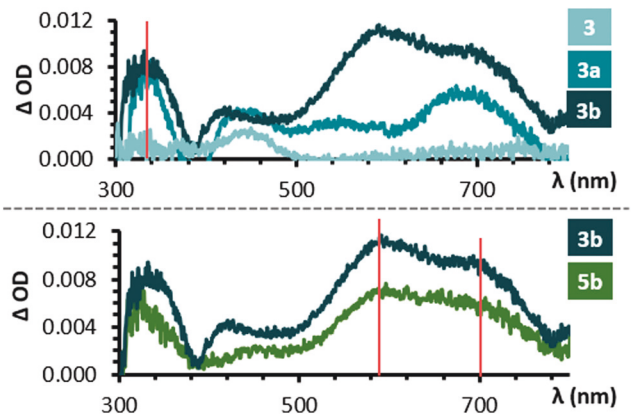

Fig. 6 Overlapping spectral absorption traces of ^{3}PC* for **3**, **3a**, and **3b** (top) as well as PCs **3b** and **5b** (bottom).

group (*i.e.* **3**, **3a**, and **3b**) we observed similar features that support the SOMOs computationally predicted by DFT (Fig. 4). For **3**, **3a**, and **3b**, a similar absorption feature of ^{3}PC* is observed at ~333 nm. We propose that this absorption feature is representative of a high energy absorption from the low lying SOMO of ^{3}PC* to some higher energy unoccupied molecular orbital ($LUMO_{+n}$). As the low lying SOMO of PCs **3**, **3a**, and **3b** are predicted to reside primarily on the core of the PC (Fig. S70†), it makes sense that the absorption features they have at ~333 nm would look similar. Furthermore, when comparing the spectral absorption traces of ^{3}PC* for **3b** and **5b**, we note two similar features at ~590 nm and ~698 nm. We propose that these lower energy transitions are representative of excitation from the higher lying SOMO on the PC core substituent to some $LUMO_{+n}$. As these PCs share the same core substituent, it seems logical that these spectral absorption features at ~590 nm and ~698 nm would be similar.

Interestingly, ESP maps of ^{3}PC* generated using DFT suggest that the electrostatic potential of **3a**, **4a**, and **5a** is, largely, shifted away from the *N*-aryl group to one side of the molecule where for **3b**, **4b**, and **5b** electron density, though also shifted away from the *N*-aryl group, is shared between all four core substituents (Fig. S73–S75†). For PC **4**, a small $\Delta\lambda$ is observed (Fig. 5A) as well as a lack of solvatochromism (Fig. 5C) and there is no observable shift in electrostatic potential between the ground state singlet PC (^{1}PC) and ^{3}PC* (Fig. 5E). Interestingly, when PC **4** is core-extended with EWG **a**, there is a measurable increase in $\Delta\lambda$ (Fig. 5B), in the extent of solvatochromism (Fig. 5D), and electrostatic potential in ^{3}PC* appears to shift from ^{1}PC* so that electron density is heavily centered across two of the core substituents rather than on the PC core (Fig. 5F). These observations suggest that core-extension can be used to modulate CT in PCs with a primary structure that does not possess CT character in the excited state.

Excited state energies. Energies of PC singlet excited states ($E_{S1,exp}$) were experimentally determined from the $\lambda_{max,em}$ measured using fluorescence spectroscopy. $E_{S1,exp}$ for core-extended DHPs ranged from 1.95 eV to 2.12 eV and was determined to be higher for all core-extended DHPs than for non-core-extended DHPs (with PC **4** *vs.* **4a** as an exception). Transitioning from EWG **a** to EDG **b** resulted in a decrease in E_{S1} by 0.17 eV for **3a** (2.12 eV) to **3b** (1.95 eV) and by 0.11 eV for **5a** (2.11 eV) to **5b** (2.00 eV). For core-extended DHPs the *N*-aryl group seems to have a smaller impact on E_{S1} than the electronics of the core substituent. $E_{S1,exp}$ for **3a** and **5a** are nearly isoenergetic and are higher than **4a** by <0.05 eV. Additionally, $E_{S1,exp}$ for **3b** and **5b** are only separated by 0.05 eV. Interestingly, core-extension of DHPs is predicted to lower the energy of the lowest energy triplet excited state ($E_{T1,comp}$) relative to the parent non-core-extended PCs. PCs **3a** ($E_{T1,comp}$ = 1.91 eV) and **3b** ($E_{T1,comp}$ = 2.07 eV) $E_{T1,comp}$ is predicted to be lower than that of the parent DHP PC (PC **3**: $E_{T1,comp}$ = 2.23 eV). The same trend is observed between PCs **5** ($E_{T1,comp}$ = 2.19 eV), **5a** ($E_{T1,comp}$ = 1.89 eV) and **5b** ($E_{T1,comp}$ = 1.99 eV) as well as for PCs **4** ($E_{T1,comp}$ = 2.29 eV) and **4a** ($E_{T1,comp}$ = 1.82 eV). For core-extended DHPs with the same core substituents, $E_{T1,comp}$ does not change by more than 0.08 eV which is within the margin of error for these calculations observed for a similar series of PCs.[19] The same is true for the parent DHPs, where no more than a 0.10 eV shift in $E_{T1,comp}$ is predicted. Interestingly, the largest changes in $E_{T1,comp}$ are between core-extended DHPs with the same *N*-aryl group, but different core substituents. For example, for PC **3b** ($E_{T1,comp}$ = 2.07 eV) core-extended with EDG **b** $E_{T1,comp}$ is predicted to be 0.16 eV higher in energy than $E_{T1,comp}$ for **3a** ($E_{T1,comp}$ = 1.91 eV), the latter of which is core-extended with EWG **a**. Our observations suggest that the electronics of the core-substituent could have more impact on $E_{T1,comp}$ than the identity of the *N*-aryl group, however an expanded study of core-extended DHPs is necessary to confirm this.

Excited state lifetimes. The excited state lifetimes (τ) of PCs are posited to have a significant role in PC reactivity as the lowest energy excited state must persist long enough to engage in a bimolecular reaction. Though there are exceptions, an excited state lifetime of >1 ns is typically considered sufficient time for the excited state molecule to engage in a bimolecular reaction. Unfortunately, without measuring quantum yield of intersystem crossing (ϕ_{ISC}), we can currently only speculate on the relative concentrations of ^{1}PC* and ^{3}PC* in our system through measuring the quantum yield of fluorescence (ϕ_f; *vide infra*), however we are able to investigate the impact of structural changes on the excited state lifetimes of core-extended and non-core-extended DHPs. Of the PCs for which we were able to measure excited state lifetimes, the singlet excited state lifetimes (τ_{S1}) ranged from 9 ns–37 ns and triplet excited state lifetimes (τ_{T1}) ranged from 0.63 μs–144 μs. For PC **3** (τ_{S1} = 9 ns; τ_{T1} = 0.63 μs), both $\tau_{S1}$and τ_{T1} are shorter than for core-extended derivatives **3a** (τ_{S1} = 17 ns; τ_{T1} = 144 μs) and **3b** (τ_{S1} = 11 ns; τ_{T1} = 42 μs). This trend could not be verified for PCs **5** due to insufficient data. In contrast to PC **3**, a decrease in τ_{S1} is observed after core-extension of PC **4** (τ_{S1} = 37 ns) to **4a** (τ_{S1} = 13 ns). When examining the effect of core substituent electronics on excited state lifetimes, we found that for PCs **3** and **5**, τ_{S1} is longer for derivatives that are core-extended with EWG **a** (PCs **3a** & **5a**: τ_{S1} = 17 ns) than with EDG **b** (PCs **3b** & **5b**: τ_{S1} = 11 ns). For PCs **3a** and **3b** the same trend is observed for ^{3}PC* where for PC **3a** τ_{T1} = 144 ns and for **3b** τ_{T1} = 42 ns. The effect of the *N*-aryl group on the excited state lifetimes of core-extended DHPs is unclear. The experimentally determined τ_{S1} of **3a** (τ_{S1} = 17 ns) and **5a** (τ_{S1} = 17 ns) are equal as well as the τ_{S1} of **3b** (τ_{S1} = 11 ns) and **5b** (τ_{S1} = 11 ns), however there is a disparity in the triplet excited state lifetimes of core-extended PCs with different *N*-aryl groups (**3b**: τ_{T1} = 42 ns; **5b**: τ_{T1} = 108 ns). Interestingly, for non-core extended DHPs, PC **4** has a significantly longer τ_{S1} than PC **3**, and a longer τ_{T1} than PC **3** and PC **5**, suggesting that the *N*-aryl group does have a significant impact on the excited state lifetimes of non-core extended DHPs. We were unable to confidently measure and report the singlet excited state lifetime (τ_{S1}) of PC **5** as it was below the detection limit of our instrument. Furthermore, we were unable to detect a triplet signal for PCs **4a** and **5a**, there-

fore a triplet excited state lifetime (τ_{T1}) is not reported for those PCs.

Quantum yield of fluorescence. There are several pathways known to compete with relaxation of a singlet excited state molecule *via* fluorescence including non-radiative decay pathways, quenching through energy transfer or electron transfer, and phosphorescence from T1. Though ϕ_f does not lend complete information regarding the contribution of the aforementioned pathways in relaxation of PC* to ^{0}PC, a low measured ϕ_f suggests that high quantum yield of intersystem crossing is possible for that PC.[11] We used fluorescence spectroscopy to experimentally determine the ϕ_f for both the core-extended and non-core extended PCs discussed in this study. On the whole, core-extension of DHPs appears to increase ϕ_f. The experimentally determined ϕ_f of PCs **3** (ϕ_f = 1.32%) and **5** (ϕ_f = 0.72%) were both lower than ϕ_f measured for the core-extended derivatives **3a** (ϕ_f = 9.00%) and **3b** (ϕ_f = 4.31%) as well as **5a** (ϕ_f = 35.0%) and **5b** (ϕ_f = 4.00%), respectively. We found that this trend also holds true for PCs **4** (ϕ_f = 23.0%) and **4a** (ϕ_f = 36.0%) which we noted have the highest ϕ_f out of the non-core-extended and core-extended DHPs, respectively. Though we did observe that ϕ_f for core-extended DHPs with EWG **a** is higher than that for core-extended PCs with EDG **b** (*i.e.* **3a** *vs.* **3b**), the ϕ_f of PC **3a** is 26% lower than **5a**, indicating there is significant variability between PCs that, though possessing the same core substituents, have different *N*-aryl groups.

Redox properties

After assessing the photophysical properties of new core-extended DHPs, we sought to examine their redox properties. The experimental singlet excited state reduction potentials $\left(E^{o*}_{S1,exp}(^2PC^{\bullet+}/^1PC^*)\right)$ for core-extended DHPs in this study range from −1.62 to −1.78 V *vs.* SCE. The $E^{o*}_{S1,exp}(^2PC^{\bullet+}/^1PC^*)$ we measured for **3a**, **3b**, **5a**, and **5b** suggest that they are slightly more reducing than the parent non-core extended analogues; however $E^{o*}_{S1,exp}(^2PC^{\bullet+}/^1PC^*)$ does not vary by more than 0.14 V *vs.* SCE. Contrary to this trend, $E^{o*}_{S1,exp}(^2PC^{\bullet+}/^1PC^*)$ of PC **4a** $\left(E^{o*}_{S1,exp}(^2PC^{\bullet+}/^1PC^*) = -1.73\,V\,vs.\,SCE\right)$ is lower (more positive) than that of PC **4** $\left(E^{o*}_{S1,exp}(^2PC^{\bullet+}/^1PC^*) = -2.5\,V\,vs.\,SCE\right.$, respectively). The experimental oxidation potentials of $^2PC^{\bullet+}$ were estimated from the $E_{1/2}$ ($^2PC^{\bullet+}/^1PC$) which was determined using CV. $E_{1/2}(^2PC^{\bullet+}/^1PC)$ for core-extended DHPs reported in this study range from 0.23 to 0.38 V *vs.* SCE. Core-extension of PCs **3** and **5** resulted in no more than a 0.17 V *vs.* SCE increase in $E_{1/2}(^2PC^{\bullet+}/^1PC)$, however core-extension of **4** ($E_{1/2}(^2PC^{\bullet+}/^1PC)$ = 0.16 V *vs.* SCE) with EWG **a** significantly decreased the stability of $^2PC^{\bullet+}$ (PC **4a**: $E_{1/2}(^2PC^{\bullet+}/^1PC)$ = 0.34 V *vs.* SCE). On the whole, core-extension of DHPs appears to destabilize $^2PC^{\bullet+}$, rendering the core-extended derivatives more oxidizing than the parent DHPs while also destabilizing E_{S1} rendering **3a**, **3b**, **5a**, and **5b** more reducing from $^1PC^*$ than the parent derivatives.

Taking a closer look at the effects of the core substituent electronics on the redox properties, we found that $E^{o*}_{S1,exp}(^2PC^{\bullet+}/^1PC^*)$ is slightly more negative for **3a** and **5a** than for **3b** and **5b**, though only by 0.06 to 0.11 V *vs.* SCE (Fig. 7). Changing the *N*-aryl group on core-extended DHPs appears to have even less impact than core-electronics on $E^{o*}_{S1,exp}(^2PC^{\bullet+}/^1PC^*)$. Interestingly, computationally predicted triplet excited state reduction potentials $\left(E^{o*}_{T1,comp}(^2PC^{\bullet+}/^3PC^*)\right)$ have an opposite trend to what was observed for $E^{o*}_{S1,exp}(^2PC^{\bullet+}/^1PC^*)$ excluding PCs **4** and **4a**. $E^{o*}_{T1,comp}(^2PC^{\bullet+}/^3PC^*)$ is predicted to be lower for core-extended PCs (*i.e.* for **3** $E^{o*}_{T1,comp}(^2PC^{\bullet+}/^3PC^*)$ = −2.13 V *vs.* SCE and for PC **3a** $E^{o*}_{T1,comp}(^2PC^{\bullet+}/^3PC^*)$ = −1.67 V *vs.* SCE). When analyzing the effects of the core substituent electronics on $E^{o*}_{T1,comp}(^2PC^{\bullet+}/^3PC^*)$, we found that $E^{o*}_{T1,comp}(^2PC^{\bullet+}/^3PC^*)$ is slightly more negative for **3b** $\left(E^{o*}_{T1,comp}(^2PC^{\bullet+}/^3PC^*) = -2.06\,V\,vs.\,SCE\right)$ and **5b** $\left(E^{o*}_{T1,comp}(^2PC^{\bullet+}/^3PC^*) = -2.00\,V\,vs.\,SCE\right)$ than for **3a** $\left(E^{o*}_{T1,comp}(^2PC^{\bullet+}/^3PC^*) = -1.67\,V\,vs.\,SCE\right)$ and **5a** $\left(E^{o*}_{T1,comp}(^2PC^{\bullet+}/^3PC^*) = -1.75\,V\,vs.\,SCE\right)$. As was observed for $E^{o*}_{S1,exp}(^2PC^{\bullet+}/^1PC^*)$ values, changing the *N*-aryl group in core-extended DHPs is predicted to have a smaller effect on $E^{o*}_{T1,comp}(^2PC^{\bullet+}/^3PC^*)$ than the changing the electronics of the core-substituent. Redox reversibility was observed for all core-

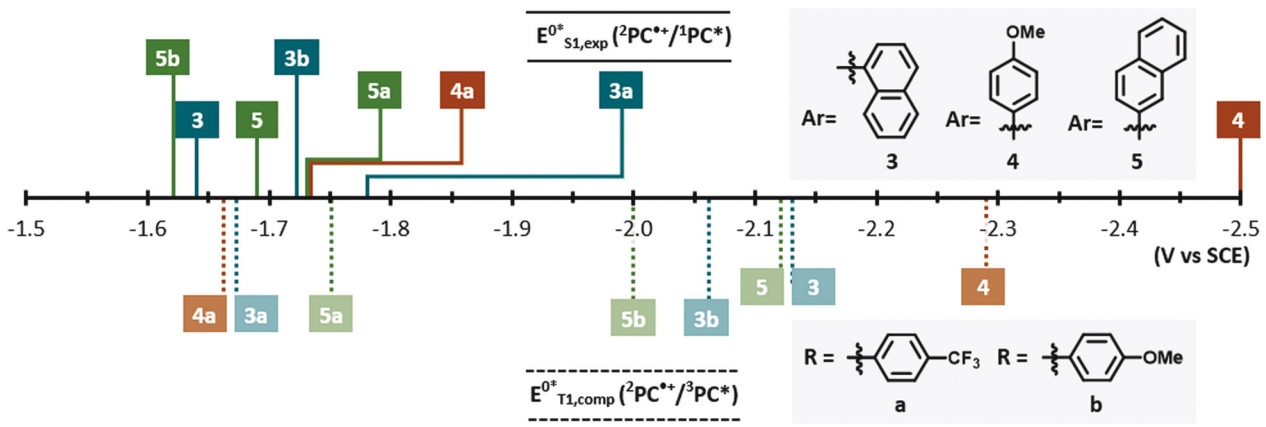

Fig. 7 (Top) Electrochemical series of experimentally measured singlet excited state redox potentials (top) and computationally predicted triplet excited state reduction potentials (bottom) of PCs investigated in this study.

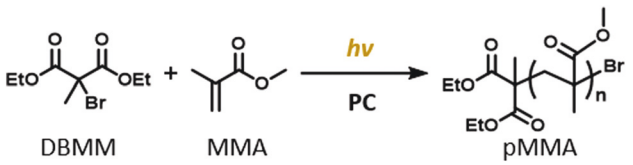

Fig. 8 General reaction scheme for the light driven polymerization of methyl methacrylate (MMA) using a photocatalyst (PC) and diethyl 2-bromo-2-methylmalonate (DBMM) as the initiator.

extended DHPs to varying degrees suggesting that they can perform as catalysts in reactions dependent on repeated reduction and oxidation reactions such as O-ATRP (Fig. S54–S60†).

O-ATRP

After investigating the structure–property relationships for the core-extended DHPs presented in this work, we sought to understand how those properties ultimately impact PC performance in O-ATRP. First, PCs were applied in the O-ATRP of methyl methacrylate (MMA) using diethyl 2-bromo-2-methylmalonate (DBMM) as the polymerization initiator and *N*,*N*-dimethylacetamide (DMAc) as the solvent (unless otherwise noted) so that [MMA] : [DMAc] : [DBMM] = [1000] : [1000] : [10] (Fig. 8 & Table 3). PC loadings were varied between 500 ppm and 10 ppm with the ppm of PC being relative to mols of monomer. All polymerizations were irradiated in a white light LED beaker and carried out under N_2. PC performance was assessed based on the degree of control with which the polymerization proceeded. Polymerization control was evaluated by first analyzing initiator efficiency (I^*) and dispersity ($Đ$). I^* is representative of the theoretical number average molecular weight ($M_{n,theo}$) divided by the observed number average molecular weight (M_n). If $I^* > 100\%$, this suggests that some of the polymer chains in the polymerization were initiated by means other than through reaction with the initiator (autoinitiation is one example). If $I^* < 100$, this suggests that initiation was inefficient due to undesirable side reactions or other processes that interfered with the polymerization of one polymer chain from one molecule of initiator. Herein, an $I^* > 90\%$ after 8 h is considered good. PC control over polymer dispersity is considered moderate if $1.3 < Đ < 1.5$, good if $1.1 < Đ < 1.3$, and excellent if $Đ < 1.1$. Additionally, PC control over the polymerization was evaluated based on the linearity of M_n growth with respect to monomer conversion throughout the polymerization and by the proximity of M_n to $M_{n,theo}$ at the same percent conversions. Polymerizations that proceeded with linear M_n growth and with M_n closer to $M_{n,theo}$ were considered to have been more controlled than polymerizations lacking those characteristics.

Previous work has demonstrated that DBMM can add to the core of parent DHP PCs resulting in a decrease in I^*.[15,16] Based on the results of previous work, we hypothesized core-extension of PCs **3**, **4**, and **5** would yield polymers with initiator efficiencies closer to unity due to the presence of core-extending substituents blocking sites on the PC core known to undergo radical addition of the initiator.[14] Indeed, the I^* in polymerizations using core-extended DHPs was typically higher than for parent DHPs, however that increase varied largely (between 1% and 42% increase in I^*). Exceptions to this trend include PC **3a** employed at 50 ppm in DMAc (Table 3, run 6) and PC **5a** employed at 500 ppm (Table 3, run 17) where polymers produced with the core-extended DHP did not have a higher I^* under the aforementioned conditions.

We too hypothesized that PCs **3a**, **3b**, **5a**, and **5b** would show increased control over the polymerization of MMA, in comparison to PCs **3** and **5**. Our reasoning stemmed from the fact that PCs **3a**, **3b**, **5a**, and **5b** have higher $\varepsilon_{max,abs}$ at a $\lambda_{max,abs}$ closer to the emission of the LEDs than PCs **3** and **5** and are equally if not more oxidizing from $^2PC^{\bullet+}$, have higher experimentally determined $E^{o*}_{S1,exp}(^2PC^{\bullet+}/^1PC^*)$, and possess CT character. To the contrary, we observed no trends suggesting that core-extended PCs consistently produce polymer with lower $Đ$ or achieve closer to unity I^* than their analogous non-core-extended DHP. In fact, we observed that between PCs **3** and **3a** and between PCs **5** and **5a**, at the same PC loadings (50 ppm and higher), $Đ$ varied by less than 0.09, except for in run 6 (Table 3) where **3a** employed at 50 ppm loading yields polymer with $Đ$ lower by 0.12 than polymer produced with **3** at 50 ppm PC loading. Overall, PCs core-extended with EDG **b** (PCs **3b** and **5b**) did not perform well in O-ATRP of MMA. For PCs **3b** and **5b**, M_n growth was not linear with respect to monomer conversion and $Đ$ stayed above 1.5 at all conversions, indicating poor control throughout the duration of the polymerization (Fig. S83, S95 & S96†). As the properties of PCs **3b** and **5b** are comparable to other core-extended DHPs that performed well, we hypothesize that the relatively lower solubility of **3b** and **5b** may hinder their efficacy in controlling the polymerization. Neither **3b** nor **5b** dissolve completely during the polymerization, thus the catalyst loading is uncertain. Furthermore, the insolubility could cause scattering of light, compromising maximum irradiation of the dissolved polymerization mixture and lowering the efficiency and uniformity of activation.

One of the most notable results we observed as a result of core-extension was that for PC **4**. Core-extension with EWG **a** to PC **4a** enabled good control in the synthesis of poly(methyl methacrylate) (PMMA) ($Đ$ = 1.27, I^* = 104%) at 50 ppm PC loading. In comparison, the parent PC to PC **4a** (PC **4**) has shown poor control at PC loadings as high as 1000 ppm ($Đ$ = 1.57, I^* = 29%).[13] To explain this observation, we reviewed three notable differences in the photophysical and electrochemical properties of PCs **4** and **4a**. First, we have shown new data to support that **4a** can access a CT excited state due to core-extension whereas PC **4** is not predicted to access a CT excited state, the former of which has been attributed as an important PC property for success in O-ATRP.[13] Second, the oxidation potential of PC **4a** ($E_{1/2}(^2PC^{\bullet+}/^1PC)$ = 0.34 V *vs.* SCE) provides more overpotential than PC **4** ($E_{1/2}(^2PC^{\bullet+}/^1PC)$ = 0.16 V *vs.* SCE) for driving deactivation in O-ATRP, the latter being essential to minimizing termination reactions during the

Table 2 Measured and predicted electrochemical properties of PCs investigated in this study

PC	$E_{1/2}$ (^{2}PC$^{\bullet+}$/^{1}PC) (V *vs.* SCE)[a]	$E^{\circ}_{ox,comp}$ (^{2}PC$^{\bullet+}$/^{1}PC) (V *vs.* SCE)[b]	$E^{\circ *}_{S1,exp}$ (^{2}PC$^{\bullet+}$/^{1}PC*) (V *vs.* SCE)[c]	$E^{\circ *}_{T1,comp}$ (^{2}PC$^{\bullet+}$/^{3}PC*) (V *vs.* SCE)[b]
3	0.23	0.10	−1.64	−2.13
3a	0.34	0.24	−1.78	−1.67
3b	0.23	0.00	−1.72	−2.06
4	0.16	0.01	−2.50	−2.29
4a	0.34	0.16	−1.73	−1.66
5	0.21[d]	0.06	−1.69	−2.12
5a	0.38	0.15	−1.73	−1.75
5b	0.38	0.00	−1.62	−2.00

[a] All measurements were performed in a 3-compartment electrochemical cell with an Ag/$AgNO_3$reference electrode in MeCN (0.01 M) and 0.1 M NBu_4PF_6 electrolyte solution. DMAc was used to solvate the PCs and in the working electrode compartment, while platinum was used as both the working and counter electrodes. E (V *vs.* SCE) = E (V *vs.* Ag/$AgNO_3$ [0.01 M]) + (0.298 V). [b] DFT calculations were performed at the uM06/6-311+G(d,p)//uM06/6-31+G(d,p) level of theory with CPCM-described solvation in DMAc. [c] Singlet excited state reduction potentials were calculated using the singlet energies (estimated from the maximum wavelength of emission) and the $E_{1/2}$. [d] Values were taken from ref. 12.

Table 3 O-ATRP results from employing PCs for the polymerization of MMA at varied catalyst loadings[a]

Run	PC	[PC][b] (ppm)	Conv.[c]	M_n [d] (kDa)	$Đ$ (M_w/M_n)[d]	I^*[e]
2	**3**	100	68%	8.97	1.07	78%
3	**3**	50	85%	8.26	1.19	105%
5	**3a**	100	65%	7.71	1.10	87%
6	**3a**	50	86%	8.80	1.07	92%
7	**3a**	10	67%	7.17	1.49	97%
8	**3b**	100	51%	5.32	1.57	101%
9	**4**[f]	1000	70%	24.7	1.57	29%
10	**4a**	100	65%	7.57	1.15	90%
11	**4a**	50	76%	7.53	1.27	104%
12	**4a**	10	67%	7.17	1.49	97%
14	**5**	100	77%	8.74	1.18	91%
15	**5**	50	87%	12.8	1.20	70%
16	**5**	10	62%	7.43	1.79	88%
18	**5a**	100	73%	8.08	1.09	93%
19	**5a**	50	80%	7.34	1.28	112%
20	**5a**	10	70%	7.54	1.42	96%
22	**5b**	100	73%	8.25	1.54	92%

[a] All polymerizations were conducted using MMA (9.35 mmol at 4.63 M) as the monomer and DBMM (0.093 mmol) as the initiator in a ratio of [1000]:[10] with DMAc as the solvent. [b] PC loading is relative to mols of monomer. [c] Conversion was determined by ^{1}H-NMR spectroscopy. [d] Measured using GPC. [e] Initiator efficiency (I^*) calculated by ((theoretical M_n/observed M_n) × 100). [f] Data obtained from ref. 12; polymerization was conducted using ethyl α-bromophenylacetate as the initiator rather than DBMM.

polymerization which compromise control. Last, the $\varepsilon_{max,abs}$ of PC **4a** ($\varepsilon_{max,abs}$ = 20 900 M^{-1} cm^{-1}) is significantly higher than for PC **4** ($\varepsilon_{max,abs}$ = 5200 M^{-1} cm^{-1}). As noted earlier, a high $\varepsilon_{max,abs}$ is posited to increase the population of ^{n}PC* enabling uniform activation,[29] however results observed from the application of PCs **3** ($\varepsilon_{max,abs}$ = 5500 M^{-1} cm^{-1}) and **5** ($\varepsilon_{max,abs}$ = 5900 M^{-1} cm^{-1}) show that polymerization control was achieved at PC loadings as low as 50 ppm despite their comparable $\varepsilon_{max,abs}$ values to PC **4**.

For PCs that yielded polymer with $Đ$ < 1.5 after 8 h of irradiation at 100 ppm PC loading (PCs **3**, **3a**, **4a**, **5**, **5a**), we proceeded to test their efficacy at even lower PC loadings (50 ppm and 10 ppm). Initially, we hypothesized that core-extended DHPs would give superior control at lower PC loadings in comparison to parent DHPs due to their high molar extinction coefficients and the blockage of sites on the PC core noted to undergo side reaction with the initiator. At 100 ppm PC **5a** outperforms PCs **3**, **3a**, **4a**, and **5**; $Đ$ remained below 1.5 at all conversions, M_n growth was linear with respect to conversion, at 8 h the initiator efficiency was closest to unity (I^* = 93%), and $Đ$ = 1.09 (Table 3, run 18) (Fig. S92†). At 50 ppm, PC **3a** outperforms PCs **3**, **4a**, **5**, and **5a** (Table 3, run 6). Although at 8 h, I^* is lower when using PC **3a** at 50 ppm (I^* = 92%) than for runs with PC **3**, **4a**, and **5a**, the run using PC **3a** is unique in that $Đ$ remained below 1.5 at all conversions and M_n growth remained linear with respect to conversion (Fig. S81†). Interestingly, for polymerizations shown in Table 3 that were run at 10 ppm PC loading, $Đ$ > 1.5 at all conversions, indicating poor control throughout the polymerization (Fig. S82, S86, S90 & S94†). Additionally, for the 10 ppm PC loading runs employing PCs **3a**, **4a**, and **5a**, PMMA only approaches the targeted M_n at high conversions—an indicator that initiation is slow. Initially, we posited that, the lack of control at 10 ppm PC loading was due to the concentration of PC being too low to afford a sufficient concentration of ^{n}PC* upon photoexcitation. Interestingly, after doing a solvent screening using PC **3a** (see discussion below) we tried applying **4a** at 10 ppm in the same polymerization conditions noted above but using benzene as the solvent instead of DMAc (Table S4,† run 33) and observed improved results in polymerization control ($Đ$ = 1.33 and I^* = 102%) compared to the run using **4a** at 10 ppm in DMAc ($Đ$ = 1.49 and I^* = 97%).

After determining that PC **3a** performed best at the lowest successful tested PC loading (50 ppm) for the polymerization of MMA in DMAc using DBMM as the initiator, we sought to assess the effect of solvent polarity on the polymerization results. Previously, several reports have shown that solvent can have a significant impact on polymerization control, especially for DHP PCs.[13,15,25] PC **3a** was used to polymerize MMA at 50 ppm PC loading in tetrahydrofuran (THF), ethyl acetate (EtOAc), benzene, and dichloromethane (DCM), in turn. Interestingly, we found that the performance of PC **3a** in the most polar solvent we tested (DMAc) ($Đ$ = 1.07, I^* = 92%) yielded nearly identical results at 8 h as the polymerization

Table 4 Solvent screening with PC **3a** for O-ATRP of MMA[a]

Run	PC	Solvent	Conv.[b]	M_n [c] (kDa)	$Đ$ (M_w/M_n)[c]	I^*[d]
6	**3a**	DMAc	86%	8.80	1.07	92%
23	**3a**	THF	78%	9.88	1.17	81%
24	**3a**	EtOAc	87%	8.79	1.23	102%
25	**3a**	Benz	89%	10.0	1.06	92%
26	**3a**	DCM	94%	8.88	1.24	109%

[a] All polymerizations were conducted using MMA (9.35 mmol at 4.63 M) as the monomer, DBMM as the initiator, and PC **3a** as the catalyst in a ratio of [1000] : [10] : [0.05]. [b] Determined by ^{1}H-NMR spectroscopy. [c] Measured using GPC. [d] Initiator efficiency (I^*) calculated by ((theoretical M_n/observed M_n) × 100).

conducted in the least polar solvent we tested (benzene) ($Đ$ = 1.06, I^* = 92%). For both of the aforementioned polymerizations (Table 4, runs 6 & 25), M_n growth was linear with respect to monomer conversion and $Đ$ < 1.5 throughout the polymerization (Fig. S81 & S99†). As observed in previous studies,[13] monomer conversion was slower in solvents of increasing polarity.

Overall, the photophysical and electrochemical properties of core-extended PCs reported in Tables 1 and 2 did not appear to significantly impact control over the polymerization of MMA through O-ATRP or their ability to control the polymerization at low ppm PC loadings >50 ppm except for comparing results obtained using PC **4**[13] *vs.* PC **4a**.

To further probe the activity of core-extended DHPs, we investigated their ability to control the polymerization of an acrylate monomer: *n*-butyl acrylate (*n*BA). The polymerization of *n*BA by O-ATRP has been a persistent challenge in the field for several reasons. First, the high rate of propagation of acrylates necessitates highly efficient deactivation to achieve a controlled polymerization ($Đ$ < 1.5). Additionally, the increased bond strength of the carbon-bromine bond at the polymer chain end of poly(*n*-butyl acrylate) (pBA) relative to PMMA[30] necessitates a greater driving force for activation relative to methacrylates. In combination, these properties of acrylate monomers and polymers require increased driving force for both activation and deactivation from PCs. Though the conditions and PCs applied for O-ATRP of *n*BA in this work did not yield polymer with $Đ$ < 1.5 (Table S4†), recent work by McCarthy *et al.* and Buss *et al.* demonstrated controlled polymerization of nBA *via* O-ATRP using alkyl core-substituted DHPs and *N*-aryl dimethyl dihydroacridines, respectively.[15,19] We hypothesize that under the conditions investigated in this study core-extended DHPs do not have sufficient driving force for enabling efficient deactivation, and thus controlled polymerization, of acrylates and other monomers with high rates of propagation.

One of the more well-studied PCs for O-ATRP is 3,7-di(4-biphenyl) 1-naphthalene-10-phenoxazine (**PhenO**). However, to the best of our knowledge, **PhenO** has not been applied in O-ATRP at PC loadings lower than 1000 ppm. **PhenO** has a comparable $\varepsilon_{max,abs}$ ($\varepsilon_{max,abs}$ = 26 600) to the PCs reported herein, absorbs at a comparable $\lambda_{max,abs}$ ($\lambda_{max,abs}$ = 388 nm), has a higher oxidation potential ($E_{1/2}(^2PC^{\bullet+}/^1PC)$ = 0.65 V *vs.* SCE), possesses CT character, has a longer triplet excited state lifetime (τ_{T1} = 480 μs), has a high ϕ_{T1} (ϕ_{T1} = 90%), and is sufficiently reducing ($E^{o*}_{S1,exp}(^2PC^{\bullet+}/^1PC^*) = -1.80$ V *vs.* SCE; $E^{o*}_{T1,comp}(^2PC^{\bullet+}/^3PC^*) = -1.70$ V *vs.* SCE) compared to core-extended DHPs.[31] To gain a better understanding of what properties might enable core-extended DHPs to work well at low ppm PC loadings, we decided to investigate **PhenO** in the O-ATRP of MMA at 50 ppm using DBMM as the initiator and DMAc as the solvent. As **PhenO** has comparable properties to core-extended DHPs, except for a higher oxidation potential (which could provide more driving force for efficient deactivation and improved polymerization control), we hypothesized that it would perform equally, if not better, in O-ATRP at a low PC loading. Interestingly, after 8 hours of polymerization, the dispersity reached using 50 ppm of **PhenO** ($Đ$ = 1.81) was higher than the dispersity of any polymer sample at 8 hours synthesized with any of the core-extended or non core-extended DHP PCs that we investigated using the same polymerization conditions ([DMAc] : [MMA] : [DBMM] = [1000] : [1000] : [10]) (Table S4,† run 34). Additionally, over the course of the polymerization M_n growth was not linear nor equivalent to $M_{n,theo}$. These data suggest that **PhenO** does not control O-ATRP of MMA under the aforementioned conditions (Fig. S105†). We also investigated the activity of **PhenO** for O-ATRP of MMA at 100 ppm and 500 ppm PC loadings. After 8 hours of polymerization using 100 ppm of **PhenO**, the observed dispersity of the polymerization mixture was $Đ$ = 1.78 and the initiator efficiency was I^* = 67% (Table S4,† run 35). After 8 hours of polymerization using 500 ppm of **PhenO**, the observed dispersity of the polymerization mixture was $Đ$ = 1.39 and the initiator efficiency was I^* = 107% (Table S4,† run 36). Despite dispersity being less than 1.5 after 8 hours of polymerization using 500 ppm of **PhenO**, throughout the polymerization M_n growth is not linear with respect to conversion and M_n is consistently >4 kDa higher than $M_{n,theo}$ The results obtained using **PhenO** at 50, 100, and 500 ppm PC loadings for the polymerization of MMA demonstrate that **PhenO** is an inferior PC relative to DHPs for controlling the polymerization of MMA in O-ATRP at low ppm PC loadings under the conditions used in this work. One potential explanation for the inferior performance of **PhenO** relative to DHPs is that the overall yield of $^1PC^*$ *vs.* $^3PC^*$ contributing to activation varies for different PCs at certain initiator concentrations.[20] If, at the concentration of DBMM used in our polymerizations, the concentration of the $^nPC^*$ species with a greater driving force for activation is higher for DHPs than it is for **PhenO**, activation with DHPs would be, comparatively, more efficient.

When considering the dispersity observed after 8 hours of polymerization and the linearity of M_n growth throughout the polymerization, PC **3a** performed the best out of the seven PCs studied herein. At 50 ppm in DMAc PC **3a** produced PMMA with $Đ$ = 1.07 after 8 hours. PC **3** performed second best at 50 ppm in DMAc yielding PMMA with $Đ$ = 1.19 after 8 hours, followed by PC **5** ($Đ$ = 1.19 at 8 hours), then by PC **4a** ($Đ$ = 1.27 at 8 hours), then PC **5a** ($Đ$ = 1.28 at 8 hours). Importantly, after

8 hours $I^* > 90\%$ for all of these runs except the one using PC **5** ($I^* = 70\%$ after 8 hours). PCs **3b** and **5b** did not produce polymer with $Đ < 1.5$ at 100 ppm PC loading and were, for that reason, not investigated in O-ATRP of MMA at 50 ppm. On the whole, further investigation into the PC properties and polymerization conditions that allow for polymerization control with PCs **3**, **5**, **3a**, **4a**, and, **5a** at low ppm PC loadings is needed.

Conclusions

In this work, we were able to successfully synthesize five new highly reducing PCs, three of which proved to be excellent PCs for controlling the polymerization of MMA at PC loadings as low as 50 ppm and 10 ppm (under certain conditions). Furthermore, we demonstrated that non-core extended DHPs can achieve satisfactory polymerization results at PC loadings as low as 50 ppm. The photophysical and electrochemical properties of the five new PCs reported here were investigated and the effects of core-extension, the electronics of the core substituents, as well as the identity and connectivity of the *N*-aryl group on PC properties were examined. We found that changing the *N*-aryl group in core-extended DHPs is predicted to have a smaller effect on predicted $\left(E^{\circ *}_{\mathrm{T1,comp}}\left({}^2\mathrm{PC}^{\bullet+}/{}^3\mathrm{PC}^*\right)\right)$ vales and experimentally determined $E^{\circ *}_{\mathrm{S1,exp}}\left({}^2\mathrm{PC}^{\bullet+}/{}^1\mathrm{PC}^*\right)$ than the changing the electronics of the core-substituent. Additionally, core-extension of DHPs appears to destabilize ${}^2\mathrm{PC}^{\bullet+}$, rendering the core-extended derivatives more oxidizing than the parent DHPs, but that overall neither changing the *N*-aryl group nor the core substituents has a significant impact on $E_{1/2}\left({}^2\mathrm{PC}^{\bullet+}/{}^1\mathrm{PC}\right)$. For PC properties relevant to photoexcitation, we found that core extension red-shifts $\lambda_{\mathrm{max,abs}}$, and significantly increases $\varepsilon_{\mathrm{max,abs}}$. For $\lambda_{\mathrm{max,abs}}$, the identity of the *N*-aryl group has a greater impact on $\lambda_{\mathrm{max,abs}}$ than the electronics of core-substituents. To the contrary, we observed that though there is a measurable change in the $\varepsilon_{\mathrm{max,abs}}$ for CE-DHPs with different *N*-aryl groups, the shifts are of a lesser magnitude than those observed when the core substituent is switched between EWG **a** and EDG **b** within PC families that have the same *N*-aryl group. In our analysis of the measured Stokes shifts for core-extended PCs, the identity of the *N*-aryl group was determined to have a smaller effect on $\Delta\lambda$ (and therefore an influence on CT) than altering the electronics of the core-substituent. We also reported experimentally determined excited state lifetimes for core-extended DHPs for the first time and found that core-extension appears to increase both τ_{S1} and τ_{T1}, that the electronics of the core have little effect on τ_{S1} but do impact τ_{T1} for **3a** and **3b**, and that changing the connectivity of the *N*-aryl naphthalene group has no effect on τ_{S1} for core-extended DHPs **3a–b** and **5a–b**, but does impact τ_{S1} for the parent DHPs and τ_{T1} for both core-extended and non-core extended DHPs. Upon investigation ϕ_{f} for the PCs reported herein, we found that ϕ_{f} is relatively low (<9%) for all DHPs discussed in this work except for **4**, **4a**, and **5a** for which ϕ_{f} was still less than 40%.

After probing the ability of DHP PCs and **PhenO** to control O-ATRP at low PC loadings, we are still uncertain as to the PC properties and polymerization conditions that facilitate control at low ppm for DHP PCs. Further investigation into PC properties such as ϕ_{ISC} and k_{a} at relevant concentrations of monomer and initiator may shed light on this.

Conflicts of interest

There are no conflicts of interest to declare.

Acknowledgements

This work was supported by Colorado State University. Research reported herein was supported by the National Science Foundation (Award 2055742) as well as Graduate Women in Science (Nell Mondy and Monique Braude Fellowships). The content presented is solely the responsibility of the authors and does not necessarily reflect the views of the funding the National Science Foundation or of Graduate Women in Science. Additionally, we acknowledge and appreciate the use of XSEDE supercomputing resources.

References

1 N. A. Romero and D. A. Nicewicz, *Chem. Rev.*, 2016, **116**, 10075–10166.
2 Y. Lee and M. S. Kwon, *Eur. J. Org. Chem.*, 2020, 6028–6043.
3 M. Chen, M. Zhong and J. A. Johnson, *Chem. Rev.*, 2016, **116**, 10167–10211.
4 N. Zivic, M. Bouzrati-zerelli, A. Kermagoret, F. Dumur, J. Fouassier, D. Gigmes and J. Lalevee, *ChemCatChem*, 2016, **8**, 1617–1631.
5 N. Corrigan, S. Shanmugam, J. Xu and C. Boyer, *Chem. Soc. Rev.*, 2016, **45**, 6165–6212.
6 B. P. Fors and C. J. Hawker, *Angew. Chem., Int. Ed.*, 2012, **51**, 8850–8853.
7 D. Konkolewicz, K. Schroder, J. Buback, S. Bernhard and K. Matyjaszewski, *ACS Macro Lett.*, 2012, **1**, 1219–1223.
8 D. Volz, M. Wallesch, C. Fléchon, M. Danz, A. Verma, J. M. Navarro, D. M. Zink, S. Bräse and T. Baumann, *Green Chem.*, 2015, **17**, 1988–2011.
9 R. M. Pearson, C. H. Lim, B. G. McCarthy, C. B. Musgrave and G. M. Miyake, *J. Am. Chem. Soc.*, 2016, **138**, 11399–11407.
10 B. G. McCarthy and G. M. Miyake, *ACS Macro Lett.*, 2018, **7**, 1016–1021.
11 B. G. McCarthy, R. M. Pearson, C. H. Lim, S. M. Sartor, N. H. Damrauer and G. M. Miyake, *J. Am. Chem. Soc.*, 2018, **140**, 5088–5101.
12 J. C. Theriot, C. H. Lim, H. Yang, M. D. Ryan, C. B. Musgrave and G. M. Miyake, *Science*, 2016, **352**, 1082–1086.

13 M. D. Ryan, J. C. Theriot, C. H. Lim, H. Yang, A. G. Lockwood, N. G. Garrison, S. R. Lincoln, C. B. Musgrave and G. M. Miyake, *J. Polym. Sci., Part A: Polym. Chem.*, 2017, **55**, 3017–3027.
14 J. P. Cole, C. R. Federico, C. H. Lim and G. M. Miyake, *Macromolecules*, 2019, **52**, 747–754.
15 B. G. McCarthy, S. Sartor, J. Cole, N. Damrauer and G. M. Miyake, *Macromolecules*, 2020, **53**, 9208–9219.
16 D. A. Corbin, K. O. Puffer, K. A. Chism, J. P. Cole, J. C. Theriot, B. G. McCarthy, B. L. Buss, C. H. Lim, S. R. Lincoln, B. S. Newell and G. M. Miyake, *Macromolecules*, 2021, **54**, 4507–4516.
17 N. A. Swisher, D. A. Corbin and G. M. Miyake, *ACS Macro Lett.*, 2021, **10**, 453–459.
18 S. M. Sartor, C. H. Chrisman, R. M. Pearson, G. M. Miyake and N. H. Damrauer, *J. Phys. Chem. A*, 2020, **124**, 817–823.
19 B. L. Buss, C. H. Lim and G. M. Miyake, *Angew. Chem.*, 2020, **59**, 3209–3217.
20 Y. M. Lattke, D. A. Corbin, S. M. Sartor, B. G. McCarthy, G. M. Miyake and N. H. Damrauer, *J. Phys. Chem. A*, 2021, **125**, 3109–3121.
21 M. Sneha, A. Bhattacherjee, L. Lewis-Borrell, I. P. Clark and A. J. Orr-Ewing, *J. Phys. Chem. B*, 2021, **125**, 7840–7854.
22 A. Bhattacherjee, M. Sneha, L. Lewis-Borrell, G. Amoruso, T. A. A. Oliver, J. Tyler, I. P. Clark and A. J. Orr-Ewing, *J. Am. Chem. Soc.*, 2021, **143**, 3613–3627.
23 D. Koyama, H. J. A. Dale and A. J. Orr-Ewing, *J. Am. Chem. Soc.*, 2018, **140**, 1285–1293.
24 D. A. Corbin, B. G. McCarthy, Z. van de Lindt and G. M. Miyake, *Macromolecules*, 2021, **54**, 4726–4738.
25 C. H. Lim, M. D. Ryan, B. G. McCarthy, J. C. Theriot, S. M. Sartor, N. H. Damrauer, C. B. Musgrave and G. M. Miyake, *J. Am. Chem. Soc.*, 2017, **139**, 348–355.
26 S. M. Sartor, Y. M. Lattke, B. G. McCarthy, G. M. Miyake and N. H. Damrauer, *J. Phys. Chem. A*, 2019, **123**, 4727–4736.
27 L. Lewis-borrell, M. Sneha, A. Bhattacherjee, I. P. Clark and A. J. Orr-Ewing, *Chem. Sci.*, 2020, **11**, 4475–4481.
28 Z. Huang, S. Xiang, Q. Zhang, X. Lv, S. Ye, R. Guo and L. Wang, *J. Mater. Chem. C*, 2018, **6**, 2379.
29 J. C. Theriot, B. G. McCarthy, C. H. Lim and G. M. Miyake, *Macromol. Rapid Commun.*, 2017, **38**, 1700040.
30 M. B. Gillies, K. Matyjaszewski, P. O. Norrby, T. Pintauer, R. Poli and P. Richard, *Macromolecules*, 2003, **36**, 8551–8559.
31 Y. Du, R. M. Pearson, C. H. Lim, S. M. Sartor, M. D. Ryan, H. Yang, N. H. Damrauer and G. M. Miyake, *Chem. – Eur. J.*, 2017, **23**, 10962–10968.